Published in final edited form as:
J Neurosci. 2013 April 17; 33(16): 6950–6963. doi:10.1523/JNEUROSCI.0277-13.2013.

Calcineurin signalling mediates activity-dependent relocation of the axon initial segment

Mark D. Evans[1], **Rosanna P. Sammons**[1], **Sabrina Lebron**[1], **Adna S. Dumitrescu**[1], **Thomas B. K. Watkins**[1], **Victor N. Uebele**[2], **John J. Renger**[2], and **Matthew S. Grubb**[1]

[1]MRC Centre for Developmental Neurobiology, King's College London, 4th Floor, New Hunt's House, Guy's Campus, London SE1 1UL, UK

[2]Department of Neurology, Merck Research Labs, West Point, PA 19486, USA

Abstract

The axon initial segment (AIS) is a specialised neuronal sub-compartment located at the beginning of the axon that is crucially involved in both the generation of action potentials and in the regulation of neuronal polarity. We recently showed that prolonged neuronal depolarisation produces a distal shift of the entire AIS structure away from the cell body, a change associated with a decrease in neuronal excitability. Here, we utilised dissociated rat hippocampal cultures, with a major focus on the dentate granule cell (DGC) population, to explore the signalling pathways underlying activity-dependent relocation of the AIS. Firstly, a pharmacological screen of voltage-gated calcium channels (VGCCs) showed that AIS relocation is triggered by activation of L-type Ca_V1 VGCCs with negligible contribution from any other VGCC subtypes. Further pharmacological analysis revealed that downstream signalling events are mediated by the calcium-sensitive phosphatase calcineurin; inhibition of calcineurin with either FK506 or cyclosporin A totally abolished both depolarisation- and optogenetically-induced activity-dependent AIS relocation. Furthermore, calcineurin activation is sufficient for AIS plasticity, as expression of a constitutively active form of the phosphatase resulted in relocation of the AIS of DGCs without a depolarising stimulus. Finally, we assessed the role of calcineurin in other forms of depolarisation-induced plasticity. Neither membrane resistance changes nor spine density changes were affected by FK506 treatment, suggesting that calcineurin acts via a separate pathway to modulate AIS plasticity. Taken together, these results emphasise calcineurin as a vital player in the regulation of intrinsic plasticity as governed by the AIS.

Introduction

Integration of neuronal input into an all-or-nothing action potential output occurs at a specialised structure located within the proximal axon of a neuron, the axon initial segment (Clark et al., 2009; Bender and Trussell, 2012; Kole and Stuart, 2012). This highly structured region is composed of a number of scaffolding and extracellular matrix proteins, along with high concentrations of voltage-gated ion channels (Grubb and Burrone, 2010a; Rasband, 2010). As the governor of the major output from a neuron the AIS is well-positioned to modulate cell excitability. Accordingly, the precise position and/or length of

Corresponding Author: Matthew S. Grubb. matthew.grubb@kcl.ac.uk.
Author Contributions: Designed research: MDE, VNU, JJR, MSG
Performed research: MDE, RPS, SL, ASD, MSG
Analysed data: MDE, RPS, SL, TBKW, MSG
Wrote the paper: MDE, MSG

Conflict of Interest: MDE, RPS, ASD, SL, TBKW & MSG declare no competing financial interests. VNU & JJR are employees of Merck and Co., Inc. and may own stock and/or stock options in the company.

Europe PMC Funders Author Manuscripts

the AIS within the axon can vary a great deal across different cell-types (Kuba et al., 2006; Fried et al., 2009), and modelling studies show that these variations can have a significant impact upon a neuron's intrinsic excitability (Kuba et al., 2006; Wang et al., 2011).

The AIS appears to be a relatively static structure at rest (Hedstrom et al., 2007); however, it also undergoes dynamic changes in its location, length and viability in response to modulation of external stimuli. Increasing the activity of dissociated hippocampal neurons for 48 h causes a distal relocation of the entire AIS structure in a change associated with decreased neuronal excitability (Grubb and Burrone, 2010b), whereas removal of input from nuclear magnocellularis neurons in the chick auditory system results in an increase in AIS length over a number of days, a neuronal change associated with increased intrinsic excitability (Kuba et al., 2010). Changes at the AIS can also act much more rapidly: in response to ischemic injury the entire AIS is degraded in a calpain-dependent manner within hours (Schafer et al., 2009).

Modulating AIS position and length may therefore be an important tool that a neuron can use to control its intrinsic excitability. It seems that a likely source of this control is the ubiquitous signalling molecule calcium: AIS relocation in dissociated hippocampal neurons relies on activation of L- (Ca_V1) or T-type (Ca_V3) voltage gated calcium channels (VGCCs; Grubb and Burrone, 2010b). While T-type VGCCs play a key role in modulating action potential dynamics (Contreras, 2006; Bender and Trussell, 2009; Dreyfus et al., 2010; Bender et al., 2012), their activation is only transient. Conversely, L-type VGCCs remain activated during long-term and low level stimuli (Lipscombe et al., 2004) and have been shown to trigger a number of plasticity mechanisms via a variety of different signalling pathways (e.g. Deisseroth et al., 2003; Wheeler et al., 2012). However, the pathways leading to AIS plasticity and the extent to which these are shared with other forms of plasticity are entirely unknown.

Here we investigate the signalling pathways mediating AIS relocation in dissociated hippocampal neurons. We show that AIS movement is mediated by activation of L-type Ca_V1 VGCCs and that subsequent downstream signalling events require the calcium-calmodulin-activated phosphatase calcineurin. Calcineurin activity is also sufficient for AIS relocation plasticity. However, this mechanism is independent from other forms of depolarisation-induced intrinsic and structural plasticity in the same neurons.

Materials and Methods

Dissociated hippocampal culture and transfections

Dissociated hippocampal neurons were prepared from Wistar rat embryos of either sex dissected in Hank's Balanced Salt Solution at embryonic day 18. Hippocampi were digested with trypsin (Worthington, 0.5 mg/ml; 15 min at 37 °C) before trituration and subsequent plating at 45,000 cells/well on 13mm glass coverslips pre-coated with poly-l-lysine at 50μg/ml (Sigma) and laminin at 40 μg/ml. Neurons were cultured at 37 °C with 5% $C0_2$ in Neurobasal medium supplemented with 1% B27, 1% foetal calf serum and 500μM Glutamax. Every 3 days thereafter, half of the media was changed with media supplemented with 2% B27 and 500 μM Glutamax. Transfections were performed using lipofectamine 2000 at either 3 DIV or 7 DIV as stated below. Unless otherwise stated, all cell-culture materials were obtained from Invitrogen.

DNA constructs

The CACaN construct was a kind gift from Eloise Hudry and Brad Hyman and has been fully described previously (Wu et al., 2010). Channelrhodopsin-2-YFP (ChR2-YFP) was a kind gift from Karl Deisserorth and drives neuronal expression of channelrhodopsin-2 using

Europe PMC Funders Author Manuscripts

the synapsin promoter. The YFP construct documented within this manuscript, which is also driven from the synapsin promoter, was created by replacing the channelrhodopsin-2-YFP coding region from ChR2-YFP with YFP alone using the AgeI and BsrgI restriction sites. EGFP-C1 NFAT3 (referred to as NFAT-GFP throughout the manuscript) was obtained from Addgene (plasmid 10961) and was deposited by Toren Finkel (see Ichida and Finkel, 2001)

Pharmacology

All pharmacological experiments were performed at 10 DIV. TTA-P2, a novel and selective T-type VGCC inhibitor was developed by and obtained from Merck and Co., Inc. All pharmacological agents (drugs) were made up as per manufacturer's instructions and added at previously described effective working concentrations to neurons in 50:50 media (containing 50% conditioned and 50% fresh media) for at least 30 min before control or depolarising treatment. Neurons subjected to either the drug or solvent control were subsequently treated with + 10 mM NaCl (control) or depolarised with + 10 mM KCl for 48 h before being fixed and immunostained (see below).

Immunostaining

Neurons were fixed in 4% paraformaldehyde (TAAB Laboratories; in 3% sucrose, 60 mM PIPES, 25 mM HEPES, 5 mM EGTA, 1 mM $MgCl_2$) for 20 min at room temperature. Cells were permeabilised for 5 min with 0.25% Triton-X100 (Sigma) before blocking for 1h in 10% goat serum (GS; Sigma). Coverslips were then placed in primary antibody, made in 2% GS, to relevant concentrations: mouse monoclonal anti-ankryinG (clone N106/36, 1:500, NeuroMab); rabbit polyclonal anti-prox1 (1:1000, Sigma); rat anti-CTIP2(1:1000, Abcam); mouse monoclonal anti-CaMKII(1:1000, Millipore) and rabbit anti-calcineurin A (1:500, Abcam) for 1 h 30 min. After subsequent washing steps, coverslips were placed in relevant secondary antibody solution (Invitrogen AlexaFluor-conjugated antibodies in 2% GS, all 1:1000) for a further hour, before further washing and mounting in MOWIOL (Calbiochem).

Imaging and analysis

All imaging and subsequent analysis were performed blind to experimental group. Neurons with AISs of obvious somatic origin were visualised under epifluorescence and imaged using a laser scanning confocal microscope (Zeiss LSM 710). Neurons were imaged with appropriate excitation and emission filters, with the pinhole set to 1AU and using a 40x oil immersion objective (Zeiss). Laser power and gain settings were adjusted to prevent signal saturation. Images were taken with 3x zoom, 512 × 512 pixels (0.138 μm/pixel) and in z-stacks with 0.5 μm steps. Z-stack images were flattened into single maximum intensity projections and imported into MATLAB computer software (Mathworks) for analysis using custom written functions (Matthew Grubb and Thomas Watkins, see Grubb and Burrone, 2010b; freely available at www.mathworks.com/matlabcentral/fileexchange/28181-ais-quantification).

In each experimental group we imaged and analysed approximately 40 neurons for AIS start, max and end positions. This *n* allowed us to detect a 5μm shift in AIS end position with 90% power based on mean ± SD for pilot experiments (G*Power, Franz Faul, Kiel University, Germany). We drew a line profile along each maximum intensity projection starting at the soma that extended down the axon, through and past the AIS. At each pixel (1 pixel = 0.138 μm) along this profile, fluorescence intensity values were averaged over a 3 × 3 pixel square centred on the pixel of interest. Averaged profiles were then smoothed using a 40-point (~5 μm) sliding mean, and normalized between 1 (maximum smoothed fluorescence, location of the AIS max position) and 0 (minimum smoothed fluorescence). AIS start and end positions were obtained at the proximal and distal axonal positions,

respectively, where the normalized and smoothed profile declined to 0.33. AIS max position was taken as the peak fluorescence of each profile.

An AIS movement index (AMI) was calculated for each neuron subjected to both drug and depolarisation using its own AIS max position (a) and the mean AIS max position for other treatment groups (drug+10mM NaCl, $\left(\bar{b}\right)$; solvent + 10mM KCl, $\left(\bar{c}\right)$ and solvent + 10mM NaCl, $\left(\bar{d}\right)$ as follows:

$$AMI = \left(a - \bar{b}\right) / \left(\bar{c} - \bar{d}\right)$$

AMI values calculated for each neuron were then subjected to a single-sample t-test vs 1 to assess AIS movement in the drug compared to solvent control. If the mean AMI was greater than or statistically indistinguishable from 1, the AIS was deemed to have moved at least as far in drug as in control; however if the mean AMI was significantly less than 1, AIS movement had been at least partially blocked. In parallel analyses, an AMI significantly less than 1 always matched a significant drug x treatment interaction when performing a non-parametric 2-way ANOVA on sample ranks with the same data set (Akritas., 1990). To establish a full block of AIS movement, the AMI values were further subjected to a single-sample t-test vs 0 with appropriate Bonferroni correction for repeated testing. If the AMI was less than or statistically the same as 0, AIS movement was deemed to be fully blocked.

Calcium Imaging

We loaded 10 DIV dissociated hippocampal neurons with the ratiometric calcium indicator fura-2-AM (Invitrogen; 5 μM) in HBS (see below) for 30 min at room temperature, followed by wash, and incubation in phenol red-free Neurobasal medium (Invitrogen) containing either DMSO (control) or 1 μM FK506 treatments (30 min at 37°C). Cells were maintained in a steady gravity-fed flow of phenol red-free Neurobasal medium (34–36 °C; maintained with an in-line heater SH-27B, Harvard Apparatus) and were allowed to equilibrate for 10 minutes before an imaging protocol began. Single z-axis images were captured for both 340 nm and 380 nm excitation wavelengths every 5 seconds using an inverted Olympus IX71 microscope, an Olympus 40× oil immersion objective and a CCD camera coupled to Slidebook software (2 × 2 pixel binning). Baseline fluorescence was established during 5 minutes of perfusion before a +10 mM KCl stimulus was washed in. Fura-2 340/380 ratios were then calculated before and during +10 mM KCl wash-in, using fluorescence intensities averaged across cell body regions of interest (ROIs) and normalised to background fluorescence.

Electrophysiology

For electrophysiological experiments, pipettes were pulled from borosilicate glass (outer diameter 1.5 mm, inner diameter 1.17 mm, Harvard Apparatus), with a resistance of 3–7 MΩ, and were filled with an internal solution (see below for individual experiment details). Recordings were obtained with a Heka EPC10/2 amplifier coupled to Patchmaster acquisition software. Signals were Bessel filtered at 10 kHz (filter 1), and 2.9 kHz (filter 2), digitised, and sampled at 25–50 kHz (20–40 μs sample interval). Fast capacitance was compensated in the on-cell configuration. After membrane rupture, at a holding voltage of −60mV, with slow capacitance compensation inactive, we used responses to a 10 mV hyperpolarisation step to estimate the series resistance (R_s) of the recording (<20 MΩ for all cells; from the current peak), and the neuron's membrane resistance (R_m; from the steady

holding current at the new voltage) and membrane capacitance (C_m; from the area under the exponentially decaying current from peak to holding).

For assessment of resting potential at 10 DIV, hippocampal neurons were treated with either DMSO + 10 mM NaCl, DMSO + 10 mM KCl or 1 μM FK506 + 10 mM KCl for at least half an hour before both neurons and media were transferred to the recording chamber. Neurons were then targeted for whole-cell patch clamping with pipettes filled with an internal solution containing (in mM): 130 K-gluconate, 10 NaCl, 1 EGTA, 0.133 $CaCl_2$, 2 $MgCl_2$, 10 HEPES, 3.5 MgATP, 1 NaGTP. Immediately on membrane rupture, resting potential was assessed and recorded at $I = 0$ in current clamp. Resting potential values and all voltages reported within this manuscript were subsequently corrected for the appropriate calculated liquid junction potential of ~−15 mV.

For assessment of L-type VGCC current density at 10 DIV, we blocked all other VGCCs. Neurons were treated with 0.15 μM ω-agatoxin-TK (to block P/Q-type VGCCs), 3 μM ω-conotoxin-GIVA (to block N-type VGCCs) and either DMSO, 1 μM FK506 or 1 μM Nifedipine for at least 30 min before recording. Due to the slow wash-out of the VGCC drugs (McCleskey et al., 1987; Sather et al., 1993; Oliveria et al., 2007), ω-agatoxin and ω-conotoxin were not included in recording media but to ensure that there was little contamination from P/Q/N-type channels neurons were used within 45 min of the pre-incubation step. Neurons were recorded in an extracellular HBS containing in mM: 136 NaCl, 2.5 KCl, 10 HEPES, 10 D-glucose, 2 $CaCl_2$, 1.3 $MgCl_2$, 22.5 tetraethylammonium (TEA), 0.05 Nickel (to block R and T-type VGCC channels) , 0.01 Tetrodotoxin and either DMSO, 1 μM FK506 or 1 μM Nifedipine. Neurons were targeted for whole-cell patch clamping with pipettes filled with an internal solution containing (in mM): 130 Cs-gluconate, 10 NaCl, 1 EGTA, 0.133 $CaCl_2$, 2 $MgCl_2$, 10 HEPES, 3.5 NaATP, 1 NaGTP, and 22.5 TEA. With slow capacitance compensated, in voltage clamp, neurons were subjected to a 250ms depolarisation from a holding voltage of −60 to −40 mV every 5s. Holding at −60 mV eliminates > 80% of R-type currents (Sochivko et al., 2003; Oliveria et al., 2007). L-type current density in each treatment was measured as the average plateau current at −40 mV in the last 10 ms of the stimulus, normalised to cell capacitance.

For assessment of R_m, hippocampal neurons were treated for 48h in either DMSO + 10 mM NaCl, DMSO + 10 mM KCl, 1 μM FK506 + 10 mM NaCl or 1 μM FK506 + 10 mM KCl before transfer to HBS containing in mM: 136 NaCl, 2.5 KCl, 10 HEPES, 10 D-glucose, 2 $CaCl_2$, 1.3 $MgCl_2$. Dentate granule cells (DGCs) were specifically targeted for whole-cell recordings with pipettes filled with potassium gluconate internal solution (see above). DGCs were identified by searching for cell morphological features: DGCs are small in comparison with other neuronal types, have a rounded cell body, and have either one or two thick dendrites emanating from their cell body (see Lee et al., 2013). R_m was assessed as described above.

Photostimulation

Dissociated hippocampal neurons were sparsely transfected with ChR2-YFP at 7 DIV. At 10 DIV neurons were prepared for photostimulation by supplementing their media for at least 2 h with a cocktail of antioxidants (3.2 μM glutathione from Fisher Scientific and 110 μM vitamin C, 100 μM Trolox, 2.3 μM vitamin E, 77 nM superoxide dismutase, 10 nm catalase; all from Sigma), blocking synaptic transmission with 2,3-dihydroxy-6-nitro-7-sulfamoyl-benzo[f]quinoxaline-2,3-dione (NBQX; from Sigma) and either adding DMSO (1:10000), 1 μM FK506, or 1μM cyclosporin A. 4-well plates containing treated media and neurons were then placed on top of Blue LEDs (Luxeon Star) with individual collimators (RS components), supported by an aluminium heat sink (Fisher Electronik) and driven by DC/DC LED drivers (RS components) by in-house software written by Andrew Lowe. Neurons

were stimulated by illumination with individual LED flashes of 5 ms duration. Flashes were given at an average of 1Hz frequency but these stimuli were grouped into bursts of 5 flashes at a frequency of 20 Hz with bursts every 5 s (see Figure 7A). After 48 h, photostimulated neurons were fixed with 4% PFA and immunostained for ankyrin-G and prox1.

NFAT-GFP

For NFAT localisation experiments, hippocampal neurons were sparsely transfected with NFAT-GFP at 7 DIV and then treated at 10 DIV with either +10 mM NaCl (control) or depolarised with +10 mM KCl for 3h. Neurons were subsequently fixed and stained for prox1 and the nuclear marker TOPRO-3. NFAT-GFP distribution was assessed in Prox1-positive neurons by tracing around the nucleus of a single plane confocal image in ImageJ and measuring the mean grey value of nuclear NFAT-GFP and cytoplasmic NFAT-GFP. Then:

$$\text{NFAT}-\text{GFP distribution} = (\text{Nucleus} - \text{Cytoplasm}) / (\text{Nucleus} + \text{Cytoplasm}).$$

Constitutively active calcineurin (CACaN)

To confirm the effectiveness of the CACaN construct, we co-transfected CACaN with NFAT-GFP at 3 DIV, fixed the neurons at 12 DIV and took single plane confocal images of construct expressing neurons.

For assessment of AIS position in neurons expressing CACaN, hippocampal neurons were sparsely transfected at 3 DIV with either synapsin-driven YFP alone (control) or YFP together with CACaN (in a 1:2 ratio). Neurons were then cultured until 12 DIV where they were fixed and immunostained for prox1 and ankyrin-G.

Dendritic spine analysis

Dissociated hippocampal neurons were sparsely transfected with synapsin-driven YFP at 7 DIV. At 10 DIV neurons were treated for 48h with either DMSO + 10 mM NaCl, DMSO + 10 mM KCl, 1 μM FK506 + 10 mM NaCl or 1 μM FK506 + 10 mM KCl before fixation and immunostaining for prox1. Secondary dendrites from DGCs were imaged with 4x zoom, 1024×1024 pixels (0.104 μm /pixel) and in z-stacks with 0.5 μm steps. Z-stacks were imported into ImageJ, where they were flattened into maximum intensity projections. NeuronJ was subsequently used to measure dendritic length and spine density was calculated from the number of spines, defined as less than 5 μM in length, counted in each region.

Statistics

AIS positional data were analysed by Graph Pad Prism software. Data-sets that were non-Normal as assessed with a D'Agostino and Pearson omnibus normality test were analysed using non-parametric tests. All tests were 2-tailed with α=0.05 unless otherwise stated.

Results

All excitatory hippocampal neuron subtypes show AIS plasticity

We previously reported that chronic depolarisation of dissociated hippocampal neurons leads to an activity-dependent relocation of the entire AIS structure (Grubb and Burrone, 2010b). As the hippocampus constitutes a heterogeneous population of neurons including many classes of excitatory and inhibitory neurons we firstly decided to investigate AIS plasticity in different classes of hippocampal cells using a simple immunostaining protocol

(Williams et al., 2011; Lee et al., 2013; see Methods). Immunostaining for dentate granule cells (DGCs), CA1 and CA3 pyramidal neurons together with the crucial AIS scaffolding protein ankyrin-G revealed population-specific differences in baseline AIS position and length, which agree well with *in vivo* data. In particular, while all excitatory neurons have their AIS close to the cell soma, AIS length in DGCs is much shorter than in pyramidal cells (Kress et al., 2010). Interestingly, all major excitatory hippocampal subtypes undergo a significant activity-dependent AIS relocation in response to +10 mM KCl depolarisation for 48 h from 10-12 DIV (Figure 1; CA1 start and max position, Mann Whitney, $p < 0.0001$, end position, $p = 0.0014$, $n = 158$; CA3 start, max and end position, Mann Whitney, $p < 0.0001$, $n = 154$; DGC start, max and end position, Mann Whitney, $p < 0.0001$, $n = 1391$). However, inhibitory neurons expressing the neurotransmitter GABA do not show this type of plasticity (Figure 1; GABA start position, Mann Whitney, $p = 0.092$, max position, $p = 0.51$, end position, $p = 0.85$, $n = 54$; Grubb and Burrone, 2010b).

Calcium entry through voltage gated L-type channels triggers AIS relocation

To reduce the variability within the hippocampal population highlighted in Figure 1, we have focussed our investigation into the signalling pathways underlying AIS plasticity on a single cell-type, the DGC. This neuronal type shows reliable AIS plasticity over numerous experiments (Figure 1; see below), shows low variability in AIS position (SD for DGC end position = 5.5 μm, vs 10.8 μm for the whole hippocampal neuron population) and has unmyelinated axons *in vivo* as is the case in dissociated culture. DGCs can also be efficiently identified by labelling for prox1, a transcription factor expressed in all DGCs and only in DGCs in dissociated embryonic hippocampal cultures (Williams et al., 2011). This is true despite prox1-expressing interneurons migrating into the cortex and hippocampus from subpallial regions (N Kessaris, personal communication); no GABA-labelled neurons in our cultures stained positively for prox1 (0/100 $GABA^+$ neurons). DGCs are also one of the only cell populations in the brain to undergo neurogenesis throughout life (Lledo et al., 2006). However after culturing neurons in the presence of the thymidine analogue BrdU to label dividing cells, no DGCs were BrdU positive (0/763 $prox1^+$ neurons), suggesting that DGCs are not continuously generated in our culture conditions.

Depolarisation-induced relocation of the AIS requires the activation of L-type and/or T-type Ca^{2+} channels (Grubb and Burrone, 2010b) suggesting that Ca^{2+} entry to the neuron is the trigger for AIS movement. We used a pharmacological approach to further delineate this signalling cascade in DGCs. A new measure, the AIS movement index (AMI) gave a single value for the effect of a particular drug on AIS relocation, (see Methods and Figure 2A for example). An AMI value of 1 means that the AIS moves as far in the presence of the drug tested as in the solvent control, whereas an AMI value of 0 means that AIS movement has been totally blocked by the drug tested.

As predicted (Grubb and Burrone, 2010b), AIS relocation in DGCs was blocked by treatment with the L-type VGCC antagonist nifedipine (1 μM; Figure 2A,C; AMI 0.20 ± 0.09, single-sample t-test, p vs 1 < 0.0001, p vs 0 = 0.028, n = 39). At this concentration, nifedipine does not block T-type channels (Lee et al., 2006). Interestingly, treatment with either the novel and specific T-type antagonist TTA-P2 (10 μM) or a low concentration of nickel (50 μM) that blocks only T- and R-type calcium channels (Magee and Johnston, 1995; Bender and Trussell, 2009) failed to prevent AIS movement (Figure 2A-C; TTA-P2, AMI = 1.33 ± 0.12, n = 40; nickel, AMI = 1.28 ± 0.13, n = 39). This suggests that T-type VGCCs are not in fact required for depolarisation-induced AIS plasticity.

To confirm that the major source of calcium for depolarisation-induced AIS relocation comes through L-type VGCCs, we simultaneously inhibited all other VGCCs. Concurrently blocking T-type, P/Q-type, N-type and R-type channels with TTA-P2 (10 μM), ω-agatoxin-

TK (0.15 μM), ω-conotoxin-GIVA (3 μM) and SNX-482 (0.5 μM) respectively failed to prevent AIS movement (Figure 2B,C; AMI = 0.75 ± 0.13, single-sample t-test, p vs 1 = 0.077, n = 39). There was a non-significant trend towards a lower magnitude of movement in this mixed-block treatment; this may suggest a small contribution from a combination of these channels but could also be due to non-specific combinatorial effects of these drugs over 48 h. Regardless, L-type channels are by far the most important voltage-gated carrier of the depolarisation-induced signal for AIS relocation.

Chronic depolarisation could theoretically exert its effects through enhanced synaptic transmission, including signalling through calcium-permeable post-synaptic receptors (Berridge et al., 2000). However, this does not contribute to depolarisation-induced AIS relocation, since simultaneous treatment with both NBQX (10 μM) and APV (50 μM) failed to block AIS plasticity (Figure 2B,C; AMI = 0.96 ± 0.19, single-sample t-test, p vs 1 = 0.81, n = 29). Finally, we also ruled out amplification of the L-type calcium signal by release from internal stores. Blockade of ryanodine receptors and IP3 receptors with 10 μM ryanodine or 20 μM 2-APB, respectively, failed to prevent AIS movement (Figure 2B,C; ryanodine, AMI = 1.36 ± 0.05, n=38; 2-APB, AMI = 1.07 ± 0.17, n=29).

Together these results suggest that calcium entry though L-type VGCCs is the only trigger for AIS relocation and that this signal is not amplified by internal stores.

Calcium signalling pathways downstream of the L-type channel

Calcium influx results in numerous signalling cascades, controlling many cellular processes and different forms of neuronal plasticity. Interestingly, calcium influx is important in another form of AIS plasticity; after ischaemic injury, activation of calpain leads to rapid degradation of the AIS (Schafer et al., 2009). However calpain is not involved in depolarisation-induced AIS relocation. Blocking calpain activity with the cell-permeable inhibitor MDL-28170, at a concentration known to inhibit excitotoxicity or injury-induced AIS loss in primary hippocampal cultures (10 μM; Brorson et al., 1995; Jordán et al., 1997; Schafer et al., 2009) failed to inhibit AIS plasticity (Figure 3; AMI = 1.00 ± 0.17, n = 38). We therefore focussed on possible calcium signalling events downstream of the L-type VGCC.

Neither blocking protein kinase A (PKA) with 10 μM Rp-CamPs (Figure 3B; AMI = 0.94 ± 0.14, single-sample t-test, p vs 1 = 0.69, n = 39), protein kinase C (PKC) with 0.5 μM bisindoylmaleimide-1 (Figure 3B; AMI = 1.19 ± 0.21, n = 24), mitogen-activated protein kinase kinase (MAPKK) with 10 μM U0126 (Figure 3B; AMI = 1.08 ± 0.14, n = 38), the p38 MAPK pathway with 1 μM SB203580 (Figure 3B; AMI = 1.50 ± 0.17, n = 39), nor phosphoinositide 3 –kinase (PI3K) with 100 nM wortmannin (Figure 3B; AMI = 0.95 ± 0.31, single-sample t-test, p vs 1 = 0.86, n = 20) caused any block in AIS relocation, suggesting that these L-type VGCC targets are not involved in AIS plasticity. However, specifically inhibiting CaMKII with 1 μM tat-CN21 caused a partial but not total block of AIS relocation (Figure 3B; AMI = 0.59 ± 0.10, single-sample t-test, p vs 1 = 0.0001, p vs 0 < 0.0001, n = 37) implying that CaMKII may contribute to AIS plasticity downstream of the L-type VGCC.

Calcineurin activation is necessary for AIS relocation

Calcineurin is a phosphatase involved in neuronal plasticity, often in processes that downregulate neuronal activity in excitatory neurons (Zeng et al., 2001; Flavell et al., 2006). In order to test the possibility that calcineurin is involved in AIS plasticity, we blocked its activity using the immunosuppressant drug FK506 (1 μM). Inhibiting calcineurin with this drug totally abolished depolarisation-induced ankyrin-G relocation in DGCs (Figure 4A;

AMI = 0.11 ± 0.06, single-sample t-test, p vs 1 < 0.0001, p vs 0 = 0.07, n = 118). It also completely blocked AIS movement in CA1 and CA3 pyramidal cells (Figure 4C; CA1, AMI = −0.36 ± 0.18, n = 40; CA3, AMI = 0.22 ± 0.14, single-sample t-test, p vs 1 < 0.0001, p vs 0 = 0.11, n = 37), showing that this effect is maintained throughout the population of hippocampal excitatory neurons. FK506 continued to block AIS relocation in DGCs even at much lower concentrations (100 nM and 10 nM), close to the ic50 for the drug (Figure 4B; 100nM FK506, AMI = 0.02 ± 0.12, single-sample t-test, p vs 1 < 0.0001, p vs 0 = 0.88, n = 40; 10nM FK506, AMI = 0.25 ± 0.11, single-sample t-test, p vs 1 < 0.0001, p vs 0 = 0.04, n = 30). Taken together, these results indicate that activation of the phosphatase calcineurin is critical for depolarisation-induced AIS plasticity in all hippocampal excitatory subtypes.

A number of important control experiments ensured that calcineurin signalling is indeed required for depolarisation-induced AIS relocation. Firstly, treatment of DGC neurons with another classical calcineurin inhibitor, cyclosporin A (CsA; 1 μM), totally blocked AIS relocation (Figure 5A,C; AMI = −0.17 ± 0.07, n = 39). In order to confirm that both FK506 and CsA were acting on calcineurin in our neurons we made use of a sparsely expressed NFAT-GFP construct. NFAT is a transcription factor which when inactive is located in the cytosol but upon direct activation by calcineurin shuttles into the nucleus (Graef et al., 1999). Importantly, inhibiting calcineurin with either 1 μM FK506 or 1 μM CsA prevented translocation of NFAT-GFP to the nucleus after 3 h of +10 mM KCl stimulation in our cultures (Figure 5B; 1-way ANOVA with Tukey's multiple comparison test, DMSO + 10 mM KCl, p < 0.0001 vs DMSO + 10 mM NaCl, 1 μM FK506+10 mM KCl and 1 μM CsA + 10 mM KCl, n = 75).

Both FK506 and CsA work indirectly by binding and sequestering immunophilins - FK506 binding protein (FKBP12) and cyclophillin respectively - required for calcineurin activity. FKBP12 is also an important component of the mTOR signalling pathway. Importantly, however, the highly specific inhibitor of FKBP12, rapamycin (1 μM) had no effect on AIS relocation in DGCs (Figure 5C; AMI = 0.83 ± 0.10, single-sample t-test, p vs1 = 0.1, n = 39). Both FK506 and CsA can also act by inhibiting the Hsp90 stress response pathway (Owens-Grillo et al., 1995); however, blockade of Hsp90 with radicicol (100 nM) had no effect on AIS movement (Figure 5C; AMI = 0.83 ± 0.17, single-sample t-test, p vs 1 = 0.30, n = 39). Finally calcineurin can act through activation of another phosphatase, PP1, via inhibition of inhibitor-1 (Groth et al., 2003). However, specific block of PP1 with tautomycetin (4 nM) also failed to prevent AIS movement (Figure 5C; AMI = 0.98 ± 0.17, single-sample t-test, p vs 1 = 0.90, n = 38). By ruling out the off-target effects of these drugs, these results show that calcineurin activation is necessary for AIS plasticity.

Calcineurin acts downstream of L-type channels

The stimuli used in these experiments result in a depolarised membrane potential, calcium influx through L-type calcium channels and AIS relocation (Grubb and Burrone, 2010b). Given the reported influence of calcineurin signalling on both leak potassium channels (Czirják et al., 2004; Li et al., 2011) and on L-type calcium channels themselves (Norris et al., 2002; Oliveria et al., 2007), it is entirely feasible that blocking calcineurin could in fact exert its effects on AIS movement via upstream mechanisms, on membrane depolarisation and/or calcium influx. In order to tease apart these possibilities we studied high potassium-evoked changes in both membrane potential and calcium influx in the presence or absence of FK506.

After treatment with +10 mM KCl, the mean resting potential of neurons was depolarised by 15.3 mV to −42.7 mV. This depolarisation was the same in neurons treated with 1 μM FK506 for 48 h, illustrating that the membrane potential change is not dependent upon

calcineurin signalling (Figure 6A; 1-way ANOVA with Tukey's multiple comparison test, DMSO +10 mM KCl vs FK506 + 10 mM KCl, P>0.05, n = 27).

We then imaged the ratiometric calcium indicator fura-2 to study calcium influx into neurons for 20 min after a +10 mM KCl stimulus. Despite a lower response to the initial stimulus, the plateau phase of the calcium response, which consists of calcium influx mostly through L-type VGCCs (data not shown) was the same in neurons treated with either DMSO or 1 μM FK506 (Figure 6B; Mann Whitney p = 0.83, n = 32). This suggests that long-term calcium entry is unaffected by calcineurin signalling. However, in order to test whether calcineurin has any effect on signalling specifically through L-type VGCCs (Norris et al., 2002; Oliveria et al., 2007) we employed a cocktail of inhibitors to isolate these channels specifically (see Methods) and then used whole-cell patch-clamp recordings to measure L-type current densities under different treatment conditions. Importantly, when neurons were stepped to and held at −40 mV, the membrane potential imposed by +10 mM KCl, there was no difference in L-type current density between DMSO-and FK506-treated neurons (Figure 6C; 1-way ANOVA with Tukey's multiple comparison test, DMSO +10 mM KCl vs FK506 + 10 mM KCl, P>0.05, n = 28). Treatment with 1 μM nifedipine blocked the majority of this current showing that the channels were reasonably well isolated with this protocol (Figure 6C).

Taken together, blocking calcineurin has no effect on the membrane depolarisation or calcium influx induced by +10 mM KCl treatment. We therefore conclude that the calcineurin activity crucial for AIS relocation is downstream of the L-type VGCC.

Calcineurin Inhibitors also block photostimulation-induced AIS relocation

Thus far we have used chronic depolarisation as a simple paradigm to induce AIS relocation, but it is important to show that the calcineurin pathway is also involved in a more physiologically relevant method of inducing this type of AIS plasticity. Chronic 48 h photostimulation of ChR2-expressing neurons with bursts of blue light has previously been shown to cause AIS relocation (Grubb and Burrone, 2010b). A slightly adapted protocol (see Methods) caused distal relocation of the AIS of channelrhodopsin-2-expressing DGCs in DMSO control conditions but this was completely blocked by treatment with either 1 μM FK506 or 1 μM Cylcosporin A (Figure 7; Kruskall Wallis with Dunn's post-test, photostimulation + DMSO vs either photostimulation + 1 μM FK506, Start $p < 0.001$, Max $p < 0.01$, End $p < 0.01$; or photostimulation + 1 μM CsA, Start $p < 0.001$, Max $p < 0.05$, End $p < 0.05$; n = 76). AIS relocation is therefore reliant upon calcineurin signalling whether induced by depolarisation or patterned chronic photostimulation.

Calcineurin activation is sufficient for AIS relocalisation

We have shown that calcineurin signalling downstream of the L-type VGCC is necessary for AIS relocation. To assess whether calcineurin signalling is also sufficient for AIS plasticity we used a constitutively active form of the phosphatase (CACaN). CACaN activity was confirmed by the nuclear localisation of co-transfected NFAT-GFP without the need for depolarisation (nuclear localisation observed in 15/15 neurons, Figure 8A). In DGCs co-transfected with CACaN and YFP at 3 DIV, AISs labelled by ankyrin-G immunostaining at 12 DIV were significantly more distal than those transfected with YFP alone (Figure 8B; YFP + CACaN vs YFP alone, start, max and end position, Mann Whitney, $p < 0.0001$, n = 104). These data show that calcineurin activation is also sufficient for AIS plasticity.

Calcineurin is not localised to the AIS

Many proteins that regulate AIS structure, function and development are concentrated within the AIS region (Grubb and Burrone, 2010a; Rasband, 2010). As calcineurin is both

necessary and sufficient for AIS relocation we wanted to assess whether there was a specific concentration of the enzyme at the AIS. Immunostaining for the catalytic subunit of calcineurin (calcineurin A) brightly labelled DGCs transfected with CACaN, showing that the antibody does recognise a calcineurin epitope (Figure 9A). Untransfected cells showed nuclear concentration of the phosphatase, with diffuse expression throughout the neurites but no AIS concentration of calcineurin in DGCs treated with 10 mM NaCl, 3 h of depolarisation (+10 mM KCl) or after 48 h depolarisation and full AIS relocation (Figure 9B). These data suggest that although its enzymatic activity effects AIS position there is no specific localisation of calcineurin at the AIS.

Calcineurin is not crucial for other forms of depolarisation-induced plasticity

Depolarisation-induced AIS relocation is a form of structural plasticity in neurons that may act to alter intrinsic excitability. We finally wanted to examine whether other forms of intrinsic and structural plasticity brought about by our chronic depolarisation stimulus were also regulated by calcineurin signalling.

Membrane resistance (R_m) in cultured hippocampal neurons has been shown to decrease after chronic depolarisation (Grubb and Burrone, 2010b; O'Leary et al., 2010). We targeted DGCs for whole-cell voltage-clamp recordings (see Methods and Figure 10A) after 48 h depolarisation from 10 or 11 DIV in the presence or absence of 1 μM FK506. As predicted, in DMSO, DGCs treated with +10 mM KCl showed decreased R_m compared to neurons treated with +10 mM NaCl. Interestingly, DGCs treated with FK506 had increased R_m in both control and depolarising treatments, but R_m still decreases in response to chronic depolarisation. This led to significant effects of treatment and drug, but no interaction between the two factors (Figure 10A; 2-way ANOVA on ranks, effect of treatment, $p < 0.001$; drug, $p = 0.025$; interaction $p = 0.133$, $n = 231$). Therefore R_m changes induced by depolarisation with +10 mM KCl are not reliant upon calcineurin signalling (Figure 10A).

Dendritic spine density can also be modulated by strong activity in a calcineurin-dependent manner (Halpain et al., 1998; Kurz et al., 2008; Tian et al., 2010). We therefore decided to investigate the effects of our low-level depolarising stimulus on the dendritic spines of DGCs. We sparsely transfected neurons with YFP at 7 DIV to reveal their morphology and measured DGC spine density from secondary dendrites after 48 h treatment with +10 mM NaCl or + 10 mM KCl. Interestingly we also observed an activity-dependent decrease in spine density (Figure 10B). However, although there was a trend towards increased baseline spine density with calcineurin blockade, a similar level of spine density loss was induced by depolarisation in both DMSO treated and FK506 treated neurons (Figure 10B; 2-way ANOVA on ranks, effect of treatment, $p < 0.0001$; drug, $p = 0.11$; interaction $p = 0.43$, $n = 180$). Whereas previous papers, which used much stronger depolarisation have shown calcineurin to be important in regulating spine density (Halpain et al., 1998; Kurz et al., 2008; Tian et al., 2010), calcineurin signalling is not required for the effect of +10 mM KCl on DGC spine density.

Together these results suggest that AIS plasticity is governed by calcineurin in a mechanism separate from other forms of depolarisation-induced intrinsic and structural plasticity.

Discussion

We have shown that AIS relocation plasticity occurs in all excitatory (DGC, CA1 and CA3) but not inhibitory hippocampal subtypes and is governed by the activation of L-type Ca_v1 VGCCs. The phosphatase calcineurin acts downstream of the L-type VGCC, totally blocking both depolarisation and optogenetically induced AIS plasticity when inhibited, and

inducing it when constitutively active. However, some other forms of depolarisation-induced plasticity are independent of this signalling pathway.

An L-type→calcineurin signalling pathway for AIS relocation

The long-term nature of activity-dependent AIS plasticity makes it an obvious target for control by Ca_V1 L-type VGCCs and calcineurin signalling. L-type VGCCs have been shown in many instances to couple electrical activity to different forms of long-term neuronal plasticity, including activity-dependent decreases in intrinsic excitability (e.g. Wu et al., 2008; O'Leary et al., 2010). They are ideally suited to this role: L-type VGCCs are predominantly located somatodendritically (Westenbroek et al., 1990; Hell et al., 1993; Pravettoni et al., 2000; Obermair et al., 2004), can be activated by low-level depolarisation, remain activated during long-term stimulation (Lipscombe et al., 2004) and recruit a number of signalling molecules which convey nuclear changes through the activation of transcription factors (e.g. Deisseroth et al., 2003; Wheeler et al., 2012).

Calcineurin is one such molecule, a phosphatase that is extremely sensitive to small changes in local calcium and whose activity faithfully tracks $[Ca^{2+}]$ increases (Kd ~ 0.05 μM; Stemmer and Klee, 1994; Graupner and Brunel, 2007; Forbes et al., 2012). Although recent data suggest that calpain can activate calcineurin in certain systems (e.g. Silverman-Gavrila et al., 2013), the lack of effect of calpain blockade here (Figure 3) suggests this indirect mechanism of calcium-dependent calcineurin activation is unlikely to operate in our neurons. Calcineurin-dependent pathways have been linked to plastic changes in synaptic strength and intrinsic excitability in various systems. For example, calcineurin is crucial for hippocampal LTD (Zeng et al., 2001), for activity-dependent K_V channel de-clustering in hippocampal pyramidal neurons (Misonou et al., 2004), for developmental synaptic and morphological changes in Xenopus tectal neurons (Schwartz et al., 2009), and for LTP and increased excitability in cerebellar Purkinje cells (Schonewille et al., 2010). A pool of calcineurin is tethered directly to the L-type VGCC through interactions with A-kinase anchoring proteins (AKAPs; Oliveria et al., 2007). Calcineurin may therefore become activated within the L-type VGCC microdomain at low calcium influx levels and faithfully follow calcium changes to modulate onward signalling controlling AIS position.

Other than calcineurin, only inhibition of one other calcium-dependent pathway had any effect on AIS plasticity: selective block of CaMKII partially decreased AIS relocation (Figure 3). This is intriguing because calcineurin and CaMKII signalling usually act antagonistically in the control of calcium-dependent processes (e.g. Lisman and Zhabotinsky, 2001; Wen et al., 2004; Graupner and Brunel, 2007; Gao et al., 2012). Perhaps CaMKII plays a supplementary role in AIS plasticity downstream of calcineurin signalling (Greer and Greenberg, 2008), or is involved in local cytoskeletal alterations necessary for physically relocating AIS components (Hund et al., 2010).

A non-local signal for AIS plasticity

The calcineurin-based signal for AIS relocation, however, is unlikely to act locally within the structure itself. While the AIS has some of the machinery required for activity-dependent plasticity, including VGCCs (Bender and Trussell, 2009; Yu et al., 2010) and a structure specialised for calcium-induced calcium release (Sánchez-Ponce et al., 2011), selective individual or combined block of the VGCC subtypes found at the AIS does not prevent AIS relocation (Fig 2; Grubb and Burrone, 2010b), nor does pharmacological inhibition of release from internal calcium stores (Fig 2). Furthermore, L-type VGCCs are crucial for activity-dependent AIS relocation but have never been functionally localised to the AIS (Bender and Trussell, 2009); instead these channels are known to predominantly distribute in the soma and proximal dendrites of hippocampal neurons (Hell et al., 1993; Pravettoni et

al., 2000; Obermair et al., 2004). In addition, we show here that calcineurin is needed for relocation of the AIS but is not at all concentrated at the structure (Fig 9). These considerations are most consistent with the trigger for AIS relocation being somatodendritic and away from its site of final effect, as is the case for some other forms of long-term plasticity (e.g.Ibata et al., 2008).

Possible downstream targets of calcineurin

The structure of calcineurin confers specificity to a relatively small number of downstream targets (Klee et al., 1998; Huai et al., 2002), many of which are transcription factors. NFATc4 (also known as NFAT3) is a major target expressed in the hippocampus (Graef et al., 1999) and is important for neurite outgrowth, synaptogenesis and neuronal development (Nguyen and Di Giovanni, 2008). Interestingly, like NFATc4 (Figure 4; Graef et al., 1999), TORC1, a mediator of dendritic growth translocates from the cytosol to the nucleus upon calcineurin-mediated dephosphorylation (Li et al., 2009). Moreover, this translocation is dependent upon L-type VGCCs (Li et al., 2009). Other direct targets of calcineurin include MEF2, a transcription factor involved in cell-survival (Mao et al., 1999), but also shown to regulate activity-dependent spine-density through NMDA and L-type VGCCs (Flavell et al., 2006). Calcineurin also mediates dephosphorylation of retinoblastoma (Rb), releasing a repressor complex which allows Calcium RESponsive Transactivator mediated transcription (Qiu and Ghosh, 2008). Acting via any of these transcription factors, somatic calcineurin activation could lead to transcriptional changes, producing axonally-concentrated proteins needed for local AIS movement mechanisms.

As the AIS is also strongly associated with a distinct cytoskeleton including a high density of actin (Nakada et al., 2003) and fasciculated microtubules (Palay et al., 1968), it would seem logical that its relocation would require cytoskeletal re-modelling. It is therefore interesting to note that calcineurin can influence actin remodelling through activation of slingshot, a pathway described in growth cone turning (Wen et al., 2007) and AMPA receptor insertion (Yuen and Yan, 2009). How it might do this in the context of AIS relocation, though, given that it is not concentrated at the structure (Figure 9), is not immediately obvious. Somatically-activated calcineurin could diffuse to the AIS, where it might induce changes in actin dynamics at low concentrations. Alternatively, calcineurin could act somatically on cytoskeletal modifying proteins, which if trafficked to the AIS could influence AIS relocation. In future experiments it will be interesting to test whether any of the above targets are involved in AIS relocation downstream of calcineurin activation.

Multiple pathways to long-term plasticity

We have shown here that calcineurin governs AIS relocation in dissociated cultures of the hippocampus. However, this does not suggest that all neuronal subtypes show this type of plasticity. In fact, it is becoming increasingly evident that different neuronal types are equipped to employ different methods of regulation at their AIS including relocation, length changes and ion channel modification (Kuba et al., 2010; Grubb et al., 2011; Kaphzan et al., 2011; Baalman et al., 2012). It will be very interesting to see whether calcineurin is at the heart of all changes at the AIS or whether this phosphatase solely regulates AIS relocation. Another intriguing question for future studies to ask is why inhibitory neurons in the hippocampus do not show AIS relocation? It is a possibility that these cells have low densities of L-type VGCCs, low expression of calcineurin, or a lack of AKAP-dependent calcineurin localisation to L-type channels. Alternatively, these cells may require an altogether different trigger for AIS movement.

Another crucial question is how ongoing activity changes lead to different forms of plasticity in the same type of neuron. Differences in the subcellular location and kinetics of various signalling pathways enable distinct spatiotemporal activity alterations to produce unique plastic outcomes (Berridge et al., 2000). However, a given neuronal response is not always produced by a unique stimulus activating a dedicated pathway. Sometimes the same signalling pathway can mediate multiple forms of plasticity – calcineurin, for example, is vital for both synaptic and morphological development in Xenopus tectal neurons (Schwartz et al., 2009), and is required for both LTP and increased intrinsic excitability in cerebellar Purkinje cells (Schonewille et al., 2010). In other cases the same alteration in activity can give rise to multiple forms of neuronal plasticity, not all dependent upon the same signalling pathway. This was the case here, where chronic moderate depolarisation produced calcineurin-dependent relocation of the AIS, but calcineurin-independent changes in membrane resistance and spine density in cultured dentate granule cells (Fig10). Interestingly, homeostatic synaptic plasticity induced by chronic optogenetic photostimulation is also independent of calcineurin signalling, and instead relies on the activation of CaMKIV (Goold and Nicoll, 2010; see also Ibata et al., 2008). It appears, then, that the pathways to long-term plasticity are modular to at least some degree, lacking a single overarching ‘programme’ that governs neuronal responses to chronic activity changes.

Therapeutic control of AIS position

The relevance of activity-dependent AIS relocation under physiological conditions is still under debate. Computational models suggest that there may not be a simple monotonic relationship between AIS position and excitability (Kuba et al., 2006; Kress et al., 2010; Wang et al., 2011; Baranauskas et al., 2013). In addition, unlike length changes, relocation of the AIS has yet to be reported under any conditions *in vivo*. Nevertheless, if the AIS is an important regulator of neuronal output, it is likely that mutations in the proteins involved in positioning or maintaining the AIS would lead to neurological abnormalities. Indeed the ankyrin-G and L-type VGCC genes contain specific risk loci for disorders including schizophrenia and bipolar disorder (O’Donovan et al., 2009). Moreover, in a mouse model of the neurodevelopmental disorder Angelman syndrome, hippocampal neurons had a longer AIS when compared to wild-type mice. This change resulted in higher neuronal excitability and these mice showed seizures and impaired motor function comparable with this disease in humans (Kaphzan et al., 2011). Although this field is in its infancy, it is likely that many more disorders associated with abnormalities in AIS location and/or size will be found. Thus, understanding the molecular mechanisms governing these types of plasticity may give insights into treatments for particular neurological diseases (Gründemann and Häusser, 2010). It will be interesting to see whether inhibition of calcineurin or its following downstream pathway will be able to regulate AIS position in such disorders.

Acknowledgments

Funding: This work was supported by a Wellcome Trust Career Development Fellowship to MSG, MRC 4-year PhD studentships to MDE, RPS & ASD, a UC Irvine MHIRT studentship to SL, and a Dravet Syndrome UK summer studentship to TBKW.

We would like to thank: Annisa Chand for assistance with dissociated hippocampal cultures; Phillip Gordon-Weeks, Britta Eickholt and Miles Houslay for provision of pharmacological agents and advice; Karl Deisseroth (ChR2-YFP), Eloise Hudry and Brand Hyman (CACaN) for providing DNA constructs; Andrew Lowe and Jana Mukanowa for construction and setup of the LED system and finally Juan Burrone for comments on the manuscript.

References

Akritas. The rank transform method in some two factor designs. J. Am. Stat. Assoc. 1990; 85:73–78.

Baalman K, Cotton J, Rasband N, Rasband M. BLAST WAVE EXPOSURE IMPAIRS MEMORY AND DECREASES AXON INITIAL SEGMENT LENGTH. J Neurotrauma. 2012

Baranauskas G, David Y, Fleidervish IA. Spatial mismatch between the Na+ flux and spike initiation in axon initial segment. Proc Natl Acad Sci USA. 2013

Bender KJ, Trussell LO. Axon initial segment Ca2+ channels influence action potential generation and timing. Neuron. 2009; 61:259–271. [PubMed: 19186168]

Bender KJ, Trussell LO. The physiology of the axon initial segment. Annu Rev Neurosci. 2012; 35:249–265. [PubMed: 22443507]

Bender KJ, Uebele VN, Renger JJ, Trussell LO. Control of firing patterns through modulation of axon initial segment T-type calcium channels. J Physiol (Lond). 2012; 590:109–118. [PubMed: 22063631]

Berridge MJ, Lipp P, Bootman MD. The versatility and universality of calcium signalling. Nat Rev Mol Cell Biol. 2000; 1:11–21. [PubMed: 11413485]

Brorson JR, Marcuccilli CJ, Miller RJ. Delayed antagonism of calpain reduces excitotoxicity in cultured neurons. Stroke. 1995; 26:1259–1266. discussion 1267. [PubMed: 7541574]

Clark BD, Goldberg EM, Rudy B. Electrogenic tuning of the axon initial segment. Neuroscientist. 2009; 15:651–668. [PubMed: 20007821]

Contreras D. The role of T-channels in the generation of thalamocortical rhythms. CNS Neurol Disord Drug Targets. 2006; 5:571–585. [PubMed: 17168743]

Czirják G, Tóth ZE, Enyedi P. The two-pore domain K+ channel, TRESK, is activated by the cytoplasmic calcium signal through calcineurin. J Biol Chem. 2004; 279:18550–18558. [PubMed: 14981085]

Deisseroth K, Mermelstein PG, Xia H, Tsien RW. Signaling from synapse to nucleus: the logic behind the mechanisms. Curr Opin Neurobiol. 2003; 13:354–365. [PubMed: 12850221]

Dreyfus FM, Tscherter A, Errington AC, Renger JJ, Shin H-S, Uebele VN, Crunelli V, Lambert RC, Leresche N. Selective T-type calcium channel block in thalamic neurons reveals channel redundancy and physiological impact of I(T)window. J Neurosci. 2010; 30:99–109. [PubMed: 20053892]

Flavell SW, Cowan CW, Kim T-K, Greer PL, Lin Y, Paradis S, Griffith EC, Hu LS, Chen C, Greenberg ME. Activity-dependent regulation of MEF2 transcription factors suppresses excitatory synapse number. Science. 2006; 311:1008–1012. [PubMed: 16484497]

Forbes EM, Thompson AW, Yuan J, Goodhill GJ. Calcium and cAMP levels interact to determine attraction versus repulsion in axon guidance. Neuron. 2012; 74:490–503. [PubMed: 22578501]

Fried SI, Lasker ACW, Desai NJ, Eddington DK, Rizzo JF 3rd. Axonal sodium-channel bands shape the response to electric stimulation in retinal ganglion cells. J Neurophysiol. 2009; 101:1972–1987. [PubMed: 19193771]

Gao Z, Van Beugen BJ, De Zeeuw CI. Distributed synergistic plasticity and cerebellar learning. Nat Rev Neurosci. 2012; 13:619–635. [PubMed: 22895474]

Goold CP, Nicoll RA. Single-cell optogenetic excitation drives homeostatic synaptic depression. Neuron. 2010; 68:512–528. [PubMed: 21040851]

Graef IA, Mermelstein PG, Stankunas K, Neilson JR, Deisseroth K, Tsien RW, Crabtree GR. L-type calcium channels and GSK-3 regulate the activity of NF-ATc4 in hippocampal neurons. Nature. 1999; 401:703–708. [PubMed: 10537109]

Graupner M, Brunel N. STDP in a bistable synapse model based on CaMKII and associated signaling pathways. PLoS Comput Biol. 2007; 3:e221. [PubMed: 18052535]

Greer PL, Greenberg ME. From synapse to nucleus: calcium-dependent gene transcription in the control of synapse development and function. Neuron. 2008; 59:846–860. [PubMed: 18817726]

Groth RD, Dunbar RL, Mermelstein PG. Calcineurin regulation of neuronal plasticity. Biochem Biophys Res Commun. 2003; 311:1159–1171. [PubMed: 14623302]

Grubb MS, Burrone J. Building and maintaining the axon initial segment. Curr Opin Neurobiol. 2010a; 20:481–488. [PubMed: 20537529]

Grubb MS, Burrone J. Activity-dependent relocation of the axon initial segment fine-tunes neuronal excitability. Nature. 2010b; 465:1070–1074. [PubMed: 20543823]

Grubb MS, Shu Y, Kuba H, Rasband MN, Wimmer VC, Bender KJ. Short- and long-term plasticity at the axon initial segment. J Neurosci. 2011; 31:16049–16055. [PubMed: 22072655]

Gründemann J, Häusser M. Neuroscience: A plastic axonal hotspot. Nature. 2010; 465:1022–1023. [PubMed: 20577202]

Halpain S, Hipolito A, Saffer L. Regulation of F-actin stability in dendritic spines by glutamate receptors and calcineurin. J Neurosci. 1998; 18:9835–9844. [PubMed: 9822742]

Hedstrom KL, Xu X, Ogawa Y, Frischknecht R, Seidenbecher CI, Shrager P, Rasband MN. Neurofascin assembles a specialized extracellular matrix at the axon initial segment. J Cell Biol. 2007; 178:875–886. [PubMed: 17709431]

Hell JW, Westenbroek RE, Warner C, Ahlijanian MK, Prystay W, Gilbert MM, Snutch TP, Catterall WA. Identification and differential subcellular localization of the neuronal class C and class D L-type calcium channel alpha 1 subunits. J Cell Biol. 1993; 123:949–962. [PubMed: 8227151]

Huai Q, Kim H-Y, Liu Y, Zhao Y, Mondragon A, Liu JO, Ke H. Crystal structure of calcineurin-cyclophilin-cyclosporin shows common but distinct recognition of immunophilin-drug complexes. Proc Natl Acad Sci USA. 2002; 99:12037–12042. [PubMed: 12218175]

Hund TJ, Koval OM, Li J, Wright PJ, Qian L, Snyder JS, Gudmundsson H, Kline CF, Davidson NP, Cardona N, Rasband MN, Anderson ME, Mohler PJ. A β(IV)-spectrin/CaMKII signaling complex is essential for membrane excitability in mice. J Clin Invest. 2010; 120:3508–3519. [PubMed: 20877009]

Ibata K, Sun Q, Turrigiano GG. Rapid synaptic scaling induced by changes in postsynaptic firing. Neuron. 2008; 57:819–826. [PubMed: 18367083]

Ichida M, Finkel T. Ras regulates NFAT3 activity in cardiac myocytes. J Biol Chem. 2001; 276:3524–3530. [PubMed: 11044444]

Jordán J, Galindo MF, Miller RJ. Role of calpain- and interleukin-1 beta converting enzyme-like proteases in the beta-amyloid-induced death of rat hippocampal neurons in culture. J Neurochem. 1997; 68:1612–1621. [PubMed: 9084433]

Kaphzan H, Buffington SA, Jung JI, Rasband MN, Klann E. Alterations in intrinsic membrane properties and the axon initial segment in a mouse model of Angelman syndrome. J Neurosci. 2011; 31:17637–17648. [PubMed: 22131424]

Klee CB, Ren H, Wang X. Regulation of the calmodulin-stimulated protein phosphatase, calcineurin. J Biol Chem. 1998; 273:13367–13370. [PubMed: 9593662]

Kole MHP, Stuart GJ. Signal processing in the axon initial segment. Neuron. 2012; 73:235–247. [PubMed: 22284179]

Kress GJ, Dowling MJ, Eisenman LN, Mennerick S. Axonal sodium channel distribution shapes the depolarized action potential threshold of dentate granule neurons. Hippocampus. 2010; 20:558–571. [PubMed: 19603521]

Kuba H, Ishii TM, Ohmori H. Axonal site of spike initiation enhances auditory coincidence detection. Nature. 2006; 444:1069–1072. [PubMed: 17136099]

Kuba H, Oichi Y, Ohmori H. Presynaptic activity regulates Na(+) channel distribution at the axon initial segment. Nature. 2010; 465:1075–1078. [PubMed: 20543825]

Kurz JE, Moore BJ, Henderson SC, Campbell JN, Churn SB. A cellular mechanism for dendritic spine loss in the pilocarpine model of status epilepticus. Epilepsia. 2008; 49:1696–1710. [PubMed: 18479390]

Lee KJ, Queenan BN, Rozeboom AM, Bellmore R, Lim ST, Vicini S, Pak DTS. Mossy Fiber-CA3 Synapses Mediate Homeostatic Plasticity in Mature Hippocampal Neurons. Neuron. 2013; 77:99–114. [PubMed: 23312519]

Lee T-S, Kaku T, Takebayashi S, Uchino T, Miyamoto S, Hadama T, Perez-Reyes E, Ono K. Actions of mibefradil, efonidipine and nifedipine block of recombinant T- and L-type Ca channels with distinct inhibitory mechanisms. Pharmacology. 2006; 78:11–20. [PubMed: 16899990]

Li H, Rao A, Hogan PG. Interaction of calcineurin with substrates and targeting proteins. Trends Cell Biol. 2011; 21:91–103. [PubMed: 21115349]

Li S, Zhang C, Takemori H, Zhou Y, Xiong Z-Q. TORC1 regulates activity-dependent CREB-target gene transcription and dendritic growth of developing cortical neurons. J Neurosci. 2009; 29:2334–2343. [PubMed: 19244510]

Lipscombe D, Helton TD, Xu W. L-type calcium channels: the low down. J Neurophysiol. 2004; 92:2633–2641. [PubMed: 15486420]

Lisman JE, Zhabotinsky AM. A model of synaptic memory: a CaMKII/PP1 switch that potentiates transmission by organizing an AMPA receptor anchoring assembly. Neuron. 2001; 31:191–201. [PubMed: 11502252]

Lledo P-M, Alonso M, Grubb MS. Adult neurogenesis and functional plasticity in neuronal circuits. Nat Rev Neurosci. 2006; 7:179–193. [PubMed: 16495940]

Magee JC, Johnston D. Characterization of single voltage-gated Na+ and Ca2+ channels in apical dendrites of rat CA1 pyramidal neurons. J Physiol (Lond). 1995; 487(Pt 1):67–90. [PubMed: 7473260]

Mao Z, Bonni A, Xia F, Nadal-Vicens M, Greenberg ME. Neuronal activity-dependent cell survival mediated by transcription factor MEF2. Science. 1999; 286:785–790. [PubMed: 10531066]

McCleskey EW, Fox AP, Feldman DH, Cruz LJ, Olivera BM, Tsien RW, Yoshikami D. Omega-conotoxin: direct and persistent blockade of specific types of calcium channels in neurons but not muscle. Proc Natl Acad Sci USA. 1987; 84:4327–4331. [PubMed: 2438698]

Misonou H, Mohapatra DP, Park EW, Leung V, Zhen D, Misonou K, Anderson AE, Trimmer JS. Regulation of ion channel localization and phosphorylation by neuronal activity. Nat Neurosci. 2004; 7:711–718. [PubMed: 15195093]

Nakada C, Ritchie K, Oba Y, Nakamura M, Hotta Y, Iino R, Kasai RS, Yamaguchi K, Fujiwara T, Kusumi A. Accumulation of anchored proteins forms membrane diffusion barriers during neuronal polarization. Nat Cell Biol. 2003; 5:626–632. [PubMed: 12819789]

Nguyen T, Di Giovanni S. NFAT signaling in neural development and axon growth. Int J Dev Neurosci. 2008; 26:141–145. [PubMed: 18093786]

Norris CM, Blalock EM, Chen K-C, Porter NM, Landfield PW. Calcineurin enhances L-type Ca(2+) channel activity in hippocampal neurons: increased effect with age in culture. Neuroscience. 2002; 110:213–225. [PubMed: 11958864]

O'Donovan MC, Craddock NJ, Owen MJ. Genetics of psychosis; insights from views across the genome. Hum Genet. 2009; 126:3–12. [PubMed: 19521722]

O'Leary T, Van Rossum MCW, Wyllie DJA. Homeostasis of intrinsic excitability in hippocampal neurones: dynamics and mechanism of the response to chronic depolarization. J Physiol (Lond). 2010; 588:157–170. [PubMed: 19917565]

Obermair GJ, Szabo Z, Bourinet E, Flucher BE. Differential targeting of the L-type Ca2+ channel alpha 1C (CaV1.2) to synaptic and extrasynaptic compartments in hippocampal neurons. Eur J Neurosci. 2004; 19:2109–2122. [PubMed: 15090038]

Oliveria SF, Dell'Acqua ML, Sather WA. AKAP79/150 anchoring of calcineurin controls neuronal L-type Ca2+ channel activity and nuclear signaling. Neuron. 2007; 55:261–275. [PubMed: 17640527]

Owens-Grillo JK, Hoffmann K, Hutchison KA, Yem AW, Deibel MR Jr, Handschumacher RE, Pratt WB. The cyclosporin A-binding immunophilin CyP-40 and the FK506-binding immunophilin hsp56 bind to a common site on hsp90 and exist in independent cytosolic heterocomplexes with the untransformed glucocorticoid receptor. J Biol Chem. 1995; 270:20479–20484. [PubMed: 7657624]

Palay SL, Sotelo C, Peters A, Orkand PM. The axon hillock and the initial segment. J Cell Biol. 1968; 38:193–201. [PubMed: 5691973]

Pravettoni E, Bacci A, Coco S, Forbicini P, Matteoli M, Verderio C. Different localizations and functions of L-type and N-type calcium channels during development of hippocampal neurons. Dev Biol. 2000; 227:581–594. [PubMed: 11071776]

Qiu Z, Ghosh A. A calcium-dependent switch in a CREST-BRG1 complex regulates activity-dependent gene expression. Neuron. 2008; 60:775–787. [PubMed: 19081374]

Rasband MN. The axon initial segment and the maintenance of neuronal polarity. Nat Rev Neurosci. 2010; 11:552–562. [PubMed: 20631711]

Sánchez-Ponce D, DeFelipe J, Garrido JJ, Muñoz A. In vitro maturation of the cisternal organelle in the hippocampal neuron's axon initial segment. Mol Cell Neurosci. 2011; 48:104–116. [PubMed: 21708259]

Sather WA, Tanabe T, Zhang JF, Mori Y, Adams ME, Tsien RW. Distinctive biophysical and pharmacological properties of class A (BI) calcium channel alpha 1 subunits. Neuron. 1993; 11:291–303. [PubMed: 8394721]

Schafer DP, Jha S, Liu F, Akella T, McCullough LD, Rasband MN. Disruption of the axon initial segment cytoskeleton is a new mechanism for neuronal injury. J Neurosci. 2009; 29:13242–13254. [PubMed: 19846712]

Schonewille M, Belmeguenai A, Koekkoek SK, Houtman SH, Boele HJ, Van Beugen BJ, Gao Z, Badura A, Ohtsuki G, Amerika WE, Hosy E, Hoebeek FE, Elgersma Y, Hansel C, De Zeeuw CI. Purkinje cell-specific knockout of the protein phosphatase PP2B impairs potentiation and cerebellar motor learning. Neuron. 2010; 67:618–628. [PubMed: 20797538]

Schwartz N, Schohl A, Ruthazer ES. Neural activity regulates synaptic properties and dendritic structure in vivo through calcineurin/NFAT signaling. Neuron. 2009; 62:655–669. [PubMed: 19524525]

Silverman-Gavrila LB, Praver M, Mykles DL, Charlton MP. Calcium, calpain, and calcineurin in low-frequency depression of transmitter release. J Neurosci. 2013; 33:1975–1990. [PubMed: 23365236]

Sochivko D, Chen J, Becker A, Beck H. Blocker-resistant Ca2+ currents in rat CA1 hippocampal pyramidal neurons. Neuroscience. 2003; 116:629–638. [PubMed: 12573706]

Stemmer PM, Klee CB. Dual calcium ion regulation of calcineurin by calmodulin and calcineurin B. Biochemistry. 1994; 33:6859–6866. [PubMed: 8204620]

Tian X, Kai L, Hockberger PE, Wokosin DL, Surmeier DJ. MEF-2 regulates activity-dependent spine loss in striatopallidal medium spiny neurons. Mol Cell Neurosci. 2010; 44:94–108. [PubMed: 20197093]

Wang L, Wang H, Yu L, Chen Y. Role of axonal sodium-channel band in neuronal excitability. Phys Rev E Stat Nonlin Soft Matter Phys. 2011; 84:052901. [PubMed: 22181462]

Wen Z, Guirland C, Ming G-L, Zheng JQ. A CaMKII/calcineurin switch controls the direction of Ca(2+)-dependent growth cone guidance. Neuron. 2004; 43:835–846. [PubMed: 15363394]

Wen Z, Han L, Bamburg JR, Shim S, Ming G, Zheng JQ. BMP gradients steer nerve growth cones by a balancing act of LIM kinase and Slingshot phosphatase on ADF/cofilin. J Cell Biol. 2007; 178:107–119. [PubMed: 17606869]

Westenbroek RE, Ahlijanian MK, Catterall WA. Clustering of L-type Ca2+ channels at the base of major dendrites in hippocampal pyramidal neurons. Nature. 1990; 347:281–284. [PubMed: 2169591]

Wheeler DG, Groth RD, Ma H, Barrett CF, Owen SF, Safa P, Tsien RW. Ca(V)1 and Ca(V)2 channels engage distinct modes of Ca(2+) signaling to control CREB-dependent gene expression. Cell. 2012; 149:1112–1124. [PubMed: 22632974]

Williams ME, Wilke SA, Daggett A, Davis E, Otto S, Ravi D, Ripley B, Bushong EA, Ellisman MH, Klein G, Ghosh A. Cadherin-9 regulates synapse-specific differentiation in the developing hippocampus. Neuron. 2011; 71:640–655. [PubMed: 21867881]

Wu H-Y, Hudry E, Hashimoto T, Kuchibhotla K, Rozkalne A, Fan Z, Spires-Jones T, Xie H, Arbel-Ornath M, Grosskreutz CL, Bacskai BJ, Hyman BT. Amyloid beta induces the morphological neurodegenerative triad of spine loss, dendritic simplification, and neuritic dystrophies through calcineurin activation. J Neurosci. 2010; 30:2636–2649. [PubMed: 20164348]

Wu WW, Chan CS, Surmeier DJ, Disterhoft JF. Coupling of L-type Ca2+ channels to KV7/KCNQ channels creates a novel, activity-dependent, homeostatic intrinsic plasticity. J Neurophysiol. 2008; 100:1897–1908. [PubMed: 18715900]

Yu Y, Maureira C, Liu X, McCormick D. P/Q and N channels control baseline and spike-triggered calcium levels in neocortical axons and synaptic boutons. J Neurosci. 2010; 30:11858–11869. [PubMed: 20810905]

Yuen EY, Yan Z. Dopamine D4 receptors regulate AMPA receptor trafficking and glutamatergic transmission in GABAergic interneurons of prefrontal cortex. J Neurosci. 2009; 29:550–562. [PubMed: 19144855]

Zeng H, Chattarji S, Barbarosie M, Rondi-Reig L, Philpot BD, Miyakawa T, Bear MF, Tonegawa S. Forebrain-specific calcineurin knockout selectively impairs bidirectional synaptic plasticity and working/episodic-like memory. Cell. 2001; 107:617–629. [PubMed: 11733061]

Europe PMC Funders Author Manuscripts

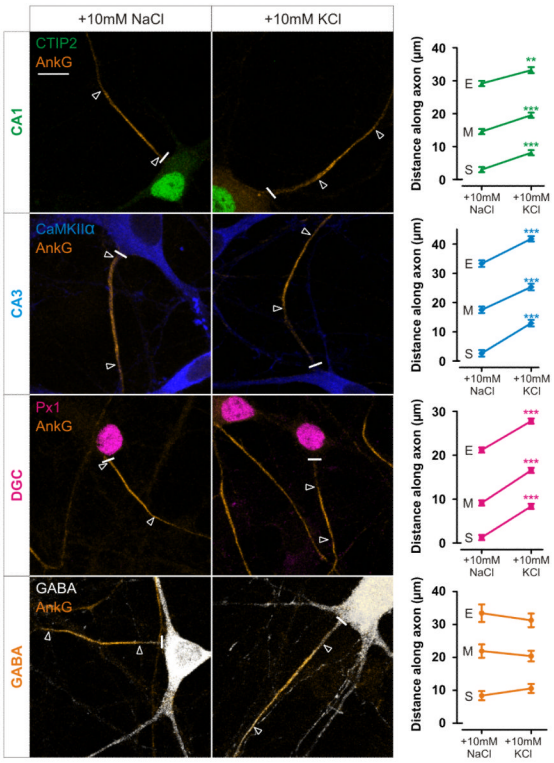

Figure 1. All excitatory hippocampal neuronal subtypes show depolarisation-induced AIS plasticity

Left: example images of DGC, CA1, CA3 and GABAergic neurons after 48 h treatment with NaCl or KCl from 10 DIV. Cell types were determined by combinatorial immunostaining (see Methods). Scale bars 10 μm; thick white line denotes axon start; white triangles illustrate AIS location. AnkG, ankyrin-G; Px1, prox1. Right: plots show mean ± SEM for AIS start (S), max (M) and end (E) position for each neuronal subtype in NaCl and KCl treatment conditions. ***, Mann Whitney test for start, max or end position, $p < 0.0001$.

Europe PMC Funders Author Manuscripts

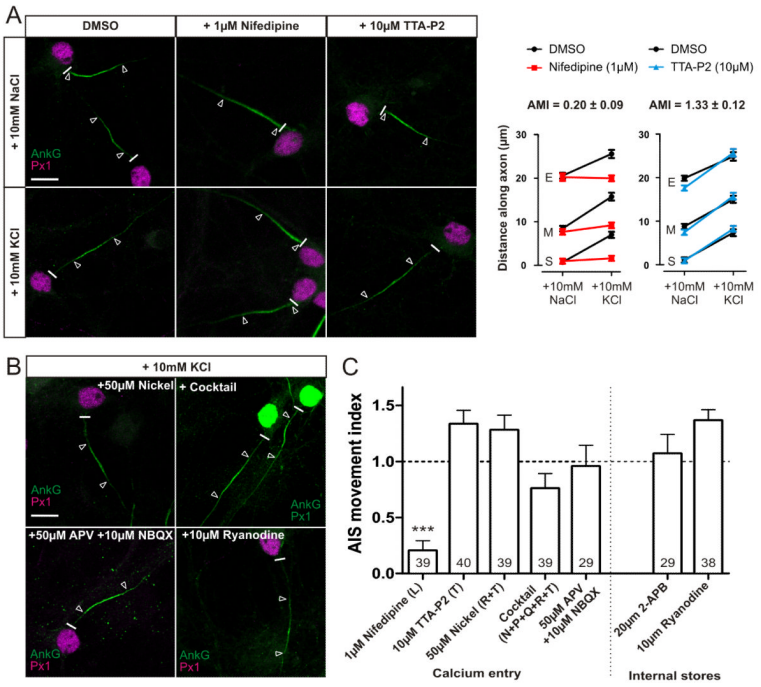

Figure 2. Only activation of L-type calcium channels is essential for AIS relocation

A) Effects of L- and T-type channel block. Left: sample images of DGCs treated with DMSO, 1 μM nifedipine or 10 μM TTA-P2 in NaCl or KCl treatment groups. Right: mean ± SEM of AIS start (S), max (M) and end (E) position for each treatment and subsequent calculation of AMI. B) Example images of DGCs treated with KCl in the presence of either: 50 μM Nickel, cocktail of VGCC inhibitors, 50 μM APV+10 μM NBQX or 10 μM ryanodine. C) AMI mean ± SEM for each drug experiment. Brackets denote VGCC subtype blocked in each experiment. ***, single sample t-test of AMI vs 1, $p < 0.0001$. Numbers within bars show the number of cells for each experiment. Scale bars 10 μm; thick white line denotes axon start; white triangles illustrate AIS location. AnkG, ankyrin-G; Px1, prox1.

Europe PMC Funders Author Manuscripts

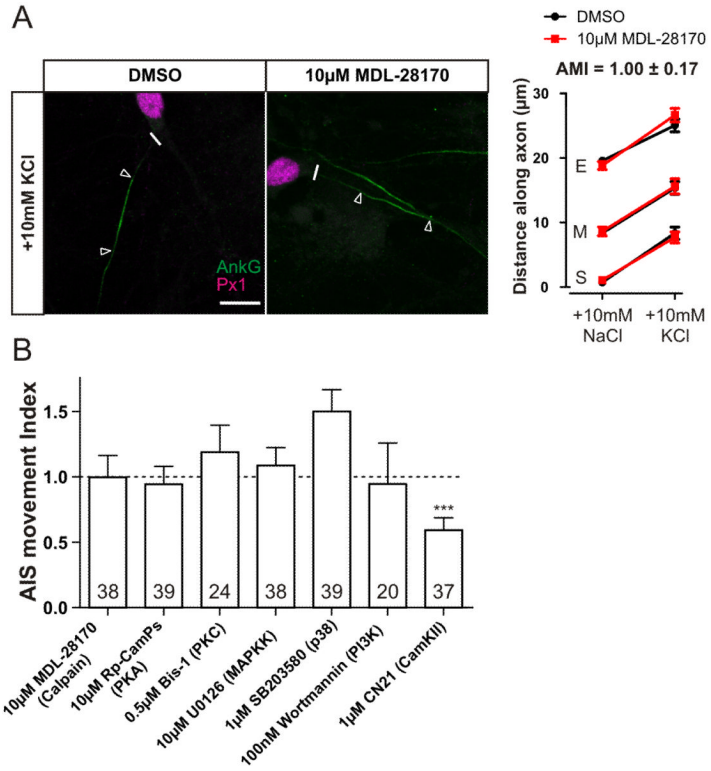

Figure 3. Screening possible calcium-activated targets downstream of L-type channels

A) Calpain is not involved in AIS relocation. Left: example images of DGCs after 48 h depolarisation in the presence of DMSO or 10 μM MDL-28170. Scale bar 10 μm; thick white line denotes axon start; white triangles illustrate AIS location. AnkG, ankyrin-G; Px1, prox1. Right: mean ± SEM of AIS start (S), max (M) and end (E) position for each treatment and subsequent calculation of AMI. B) AMI mean ± SEM for possible downstream calcium-activated targets. ***, single sample t-test of AMI vs 1, p = 0.0001. Numbers within bars show the number of cells for each experiment.

Europe PMC Funders Author Manuscripts

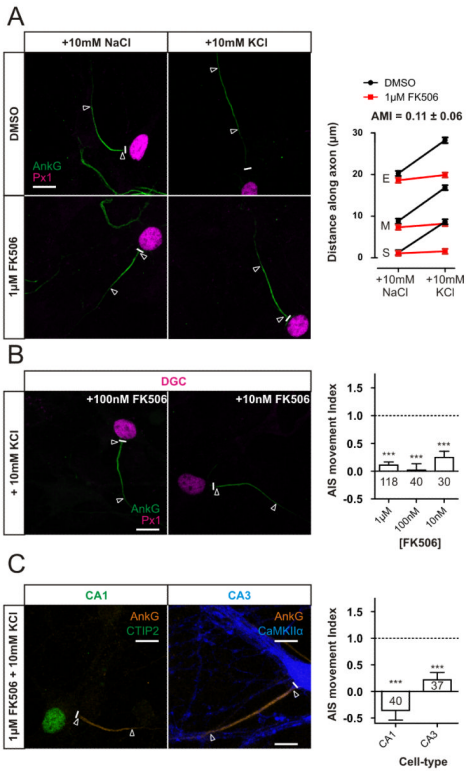

Figure 4. Calcineurin inhibition with FK506 totally blocks AIS relocation in all excitatory cell types

A) 1 μM FK506 totally inhibits DGC AIS relocation. Left: example images of DGCs treated with DMSO or 1 μM FK506 in NaCl or KCl treatment groups. Right: mean ± SEM of AIS start (S), max (M) and end (E) for each treatment and subsequent calculation of AMI. B) FK506 inhibits AIS relocation even at low concentrations. Left: example images of DGCs depolarised for 48 h in the presence of either 100 nM or 10 nM FK506. Right: AMI mean ± SEM values for DGCs after FK506 treatment. C) 1 μM FK506 blocks AIS relocation in other excitatory cell types. Left: example images of CA1 and CA3 neurons depolarised for 48 h in the presence of 1 μM FK506. Right: AMI mean ± SEM values for CA1 and CA3 neurons after FK506 treatment. ***, single sample t-test of AMI vs 1, $p < 0.0001$. Numbers within bars show the number of cells for each experiment. Scale bars 10 μm; thick white line denotes axon start; white triangles illustrate AIS location. AnkG, ankyrin-G; Px1, prox1.

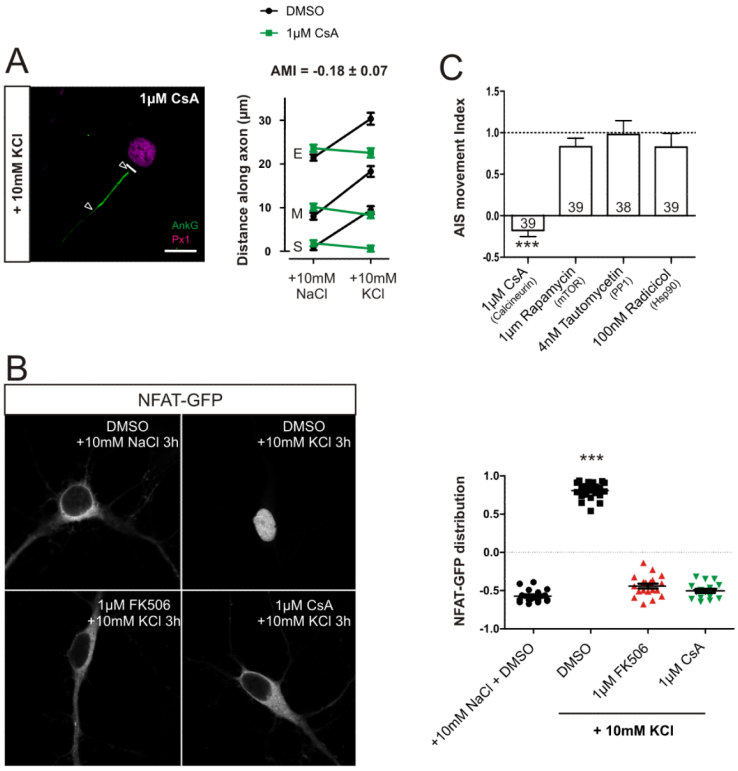

Figure 5. Inhibition of AIS relocation by FK506 is not a result of non-specific effects

A) Calcineurin inhibition by cyclosporin A totally blocks AIS movement. Left: example image of a DGC depolarised for 48 h in the presence of 1 μM cyclosporin A. Scale bar 10 μm; thick white line denotes axon start; white triangles illustrate AIS location. AnkG, ankyrin-G; Px1, prox1; CsA, cyclosporin A. Right: mean ± SEM of AIS start (S), max (M) and end (E) position for each treatment and subsequent calculation of AMI. B) Both 1 μM FK506 and 1 μM cyclosporin A block nuclear translocation of NFAT-GFP after 3 h depolarisation. Left: sample images of NFAT-GFP localisation from each treatment group. Right: NFAT-GFP nucleus/cytoplasm distribution in each treatment group. *** 1-way ANOVA with Tukey's multiple comparison test, $p < 0.0001$. C) AMI mean ± SEM values for pharmacological experiments used to test calcineurin inhibitor secondary effects. ***, single sample t-test of AMI vs 1, $p < 0.0001$. Numbers within bars show the number of cells for each experiment.

Europe PMC Funders Author Manuscripts

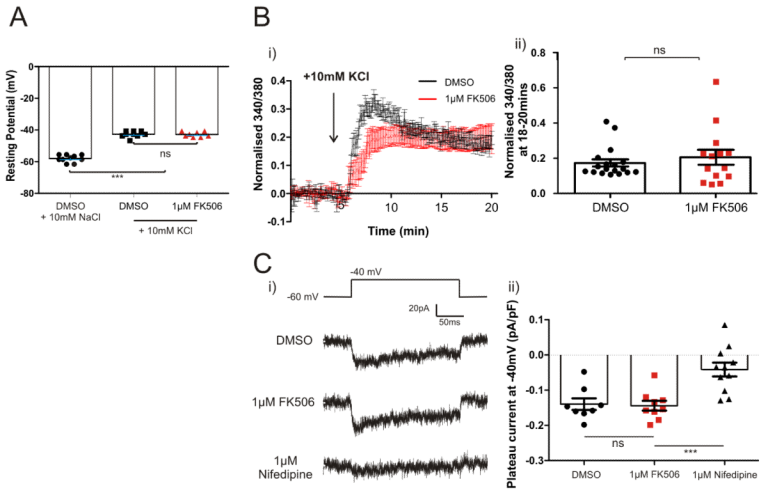

Figure 6. Calcineurin activation is downstream of L-type VGCCs

A) Calcineurin activity does not affect KCl-induced depolarisation. Resting membrane potential of neurons treated for 48 h with DMSO (black) or 1 μM FK506 (red) in NaCl or KCl treatment groups. ***, 1-way ANOVA with Tukey's multiple comparison test, $p < 0.0001$. B) Left: mean ± SEM of normalised 340/380 ratio of fura-2 ratiometric dye after depolarisation with KCl. Right: mean plateau value of normalised 340/380 ratio between 18-20 min post wash-in. Points show individual cells treated with DMSO (black) or FK506 (red). Bars show mean ± SEM of all cells in each treatment group. C) Calcineurin activity does not affect calcium influx through L-type VGCCs in neurons depolarised to −40 mV. Left: example traces of isolated L-type VGCCs in each treatment group. Thick white bar shows mean during last 10 ms of depolarising step. Right: plateau current density of isolated L-type VGCCs at −40 mV during the last 10 ms of the depolarising step in each treatment group. Points show mean of 2-5 repeats from individual neurons. Bars show mean ± SEM of all cells recorded. ***, 1 way ANOVA with Tukey's multiple comparison test, $p < 0.0001$.

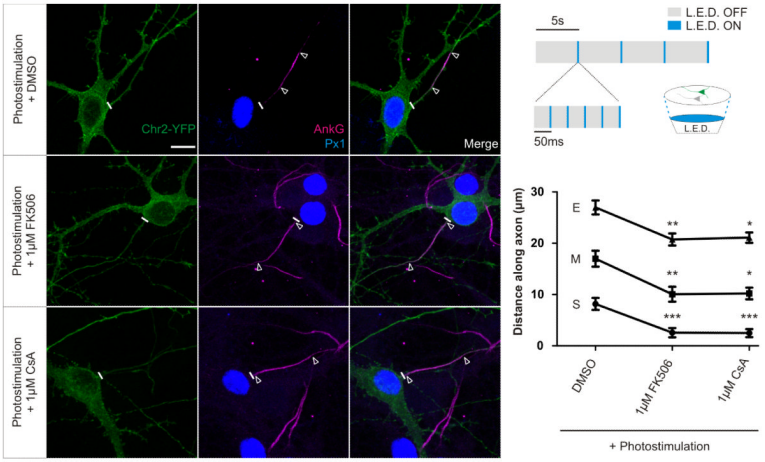

Figure 7. Photostimulation-induced AIS relocation is blocked by calcineurin inhibitors

Top right: cartoon of LED setup and stimulation paradigm. Left: example images of channelrhodopsin-2-expressing DGCs subjected to 48 h photostimulation in the presence of DMSO, 1 μM FK506 or 1 μM cyclosporin A. Scale bar 10 μm; thick white line denotes axon start; white triangles illustrate AIS location. ChR2, channelrhodopsin-2; AnkG, ankyrin-G; Px1, prox1. Bottom right: mean ± SEM of AIS start (S), max (M) and end (E) position for channelrhodpsin-2-expressing DGCs photostimulated in each treatment. Kruskall Wallis test with Dunn's multiple comparison for start, max and end positions vs DMSO, ***, $p < 0.001$;**, $p < 0.01$; *, $p < 0.05$.

Europe PMC Funders Author Manuscripts

Europe PMC Funders Author Manuscripts

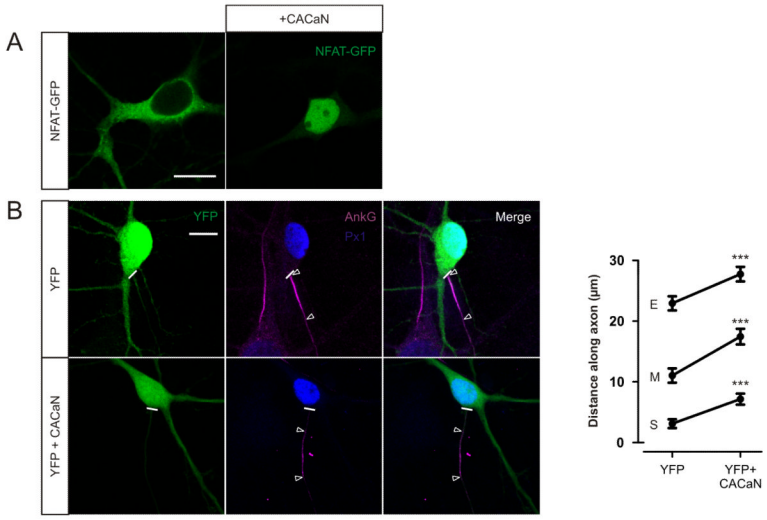

Figure 8. Calcineurin activation is sufficient for AIS relocation

A) CACaN expression causes nuclear translocation of NFAT-GFP. Left: Example image of a 12 DIV neuron expressing NFAT-GFP alone. Right: Example image of a 12 DIV neuron co-expressing NFAT-GFP and CACaN. Scale bar 10 μm. B) CACaN expression causes AIS relocation. Left: example images of DGCs at 12 DIV after 3 DIV transfection of neurons with YFP (top) or YFP + CACaN (bottom). Scale bar 10 μm, thick white line denotes axon start; white triangles illustrate AIS location. AnkG, ankyrin-G; Px1, prox1. Right: mean ± SEM of AIS start (S), max (M) and end (E) position for each group.***, Mann Whitney test for start, max or end position, $p < 0.0001$.

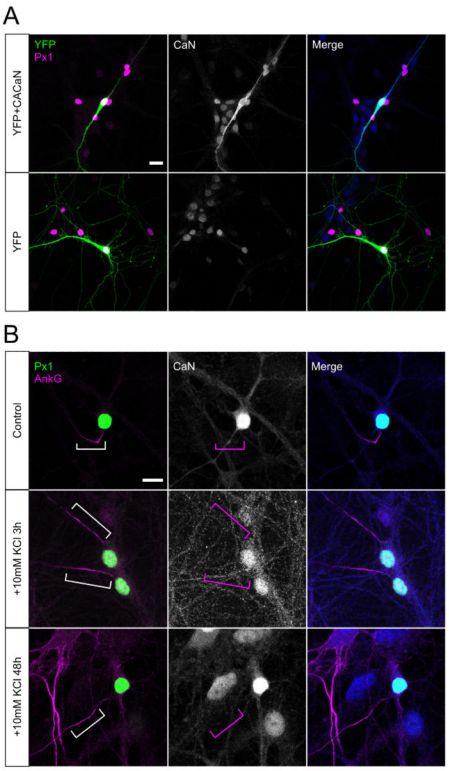

Figure 9. Calcineurin is not concentrated at the AIS

A) Example DGCs transfected with either CACaN + YFP (top) or YFP alone, labelled for calcineurin A (bottom). Scale bar 20 μm. B) Example DGCs in control conditions (top), or depolarised with KCl for 3 h (middle), or 48 h (bottom). Scale bar 10 μm. Brackets outline AIS location; note the lack of calcineurin staining in this region in all treatment groups. AnkG, ankyrin-G; Px1, prox1; CaN, calcineurin.

Europe PMC Funders Author Manuscripts

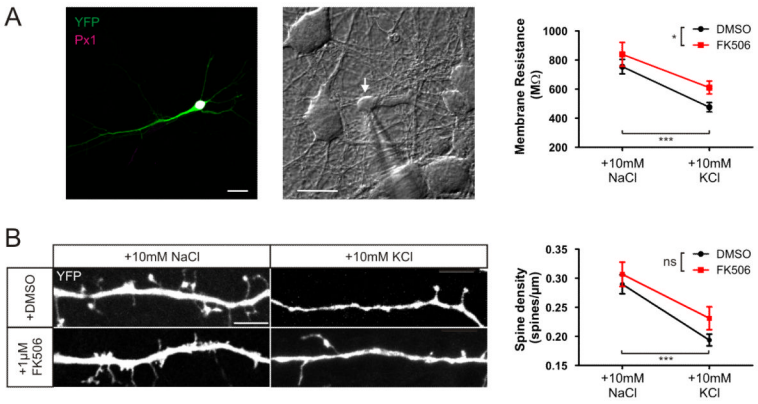

Figure 10. Calcineurin does not regulate +10 mM KCl depolarisation-induced plasticity of membrane resistance or dendritic spine density

A) Membrane resistance. Left: example DGC expressing YFP. Px1, Prox1. Middle: example image of a DGC (white arrow) targeted for whole-cell patch clamp recordings. Scale bars 20 μm. Right: mean ± SEM of membrane resistance in DGCs treated with NaCl or KCl in the presence of either DMSO (black) or 1 μM FK506 (red). B) Dendritic spine density. Example images of secondary dendrites of YFP-expressing DGCs treated with NaCl or KCl in the presence of either DMSO or 1 μM FK506. Right: mean ± SEM of dendritic spine density in each treatment group.

Europe PMC Funders Author Manuscripts